Journal of Non-Crystalline Solids 428 (2015) 176–183

Contents lists available at ScienceDirect

Journal of Non-Crystalline Solids

journal homepage: www.elsevier.com/ locate/ jnoncrysol

Electronic structure and optical properties of amorphous GeO_2 in comparison to amorphous SiO_2

Benjamin Walker, Chamila C. Dharmawardhana, Naseer Dari, Paul Rulis, Wai-Yim Ching *

Department of Physics and Astronomy, University of Missouri-Kansas City, Kansas City, MO 64110, USA

ARTICLE INFO

Article history:
Received 10 June 2015
Received in revised form 13 August 2015
Accepted 14 August 2015
Available online 31 August 2015

Keywords:
Amorphous GeO_2;
Amorphous SiO_2;
Random network models;
Electronic structure;
Optical properties

ABSTRACT

Amorphous germania (a-GeO_2) is an excellent glass former of great industrial and scientific importance. However, in comparison with a-SiO_2, its structure and fundamental properties were less well studied. Using a large near-perfect continuous random network (CRN) model with 1296 atoms and no over- or under-coordinated atoms, we have investigated the structural, electronic, and optical properties of a-GeO_2 glass. Our results show that the bond length and bond angle distributions in a-GeO_2 are larger than in a-SiO_2. The gross features of the electronic density of states in a-GeO_2 are similar to a-SiO_2, but the Ge—O bonds are weaker than Si—O bonds as reflected in the lower calculated total bond order density. The average tetrahedral angle (θ) and bridging angle (φ) are smaller in a-GeO_2 than in a-SiO_2. The calculated optical absorption spectrum shows two distinctive peaks in excellent agreement with experiment. The calculated refractive index of a-GeO_2 ($n = 1.69$) is also in close agreement with the measured value. In contrast to a-SiO_2, there is no clear evidence of excitonic peak in a-GeO_2. These a-GeO_2 and a-SiO_2 models could be used as a prototype for other investigations of these glasses or their mixtures containing defects, substitutional impurities and in the form of vitreous nano-particles.

1. Introduction

Amorphous GeO_2 (germania or a-GeO_2) is a very good glass former, similar to silica (a-SiO_2) and amorphous boron oxides [1]. It is structurally analogous to silica which has SiO_4 tetrahedral units connected with bridging O at the corners. In other words, the short range order (SRO) in a-GeO_2 and a-SiO_2 is the same as in their crystalline counterparts [1]. Good glass formers have vast technological applications in optics, semiconductors, and many other areas. The application of Germania especially in fiber optic has been fairly well-known. A more recent account is given by Dianov and Mashinsky [b2] and the references cited therein. Recently, its utilization as a photoluminescent biomimetic composite glass has been demonstrated [3]. Germania glass exhibits a lower glass transition temperature T_g (~790 K) than SiO_2 based glasses [4]. a-GeO_2 is transparent in the near infrared region and its high refractive index (n) allows for the fabrication of highly photorefractive planar waveguides which has smaller absorption losses in the middle IR range when compared to silica glass [5,6]. Therefore, understanding the electronic structure and optical properties of a-GeO_2 is of paramount importance for furthering its use in advanced applications.

It is well-known that the structure of a-SiO_2 or a-GeO_2 consists of a continuous random network (CRN) of rigid $(AO_{1/2})_4$ (A = Ge, Si) tetrahedral units connected through flexible, bridging A—O—A bonds [1]. The local SRO is usually characterized by the tetrahedral O—A—O angle (θ) and the A—O—A bridging angle (φ). Despite the similarities between CRNs of a-SiO_2 and a-GeO_2, the structure of the latter is much less studied experimentally and theoretically. To investigate the structural details and to simulate different experimental conditions, realistic atomistic models are necessary. Because amorphous glasses have no long range order (LRO), such models must use periodic boundary conditions with a sufficiently large cell to simulate an infinite random network. However, imposing periodic boundary conditions on a directionally bonded network while maintaining the approximate SRO is not an easy task. Most structural models for a-SiO_2 are either in the form of large clusters, or they are generated by using classical molecular dynamics (MD) or Monte Carlo (MC) techniques [1]. The cluster models suffer from the presence of free surfaces which complicates the analysis [7,8]. Conversely, MD/MC models always contain defective structures of under-coordinated or over-coordinated Si and O atoms and have much larger bond length and bond angle distortions [9]. The presence of such defect structures could result in the presence of undesirable states in the band gap making interpretation of experimental data more challenging. Previously, we have constructed a nearly perfect CRN model of a-SiO_2 with a 1296-atom periodic cell and have investigated its electronic, vibrational, optical and mechanical properties including the effect of densification [9–12]. Here, we adopt this model as a starting point and used it to investigate the electronic structure and optical properties of a-GeO_2.

The outline of this paper is as follows. We first describe the method of calculation and model construction for a-GeO_2 in the following section. The main results on the structure, electronic and optical

* Corresponding author.

http://dx.doi.org/10.1016/j.jnoncrysol.2015.08.018
0022-3093/

properties are presented and discussed in Section 3. In particular, we discuss the simulation of the presence of the excitonic peak in the optical spectra for a-SiO_2 and show that its inclusion can improve the calculated refractive index n. The paper ends with a brief conclusion and the vision for further study on a-GeO_2 and a-SiO_2 glasses using this large CRN model.

2. Computational method and model construction for a-GeO_2

The calculations in the present work used a two-step process. The previously used 1296-atom periodic model for a-SiO_2 is converted to an a-GeO_2 model by replacing Si with Ge and then fully optimizing the model without any constraints on cell shape or volume by using the highly accurate Vienna Ab initio Simulation Package (VASP), a density functional theory (DFT)-based method [13,14]. The electronic structure, bonding and optical properties are investigated by using the orthogonalized linear combination of atomic orbitals (OLCAO) method [15,16] using the VASP-relaxed structure. The combination of the OLCAO and VASP has proved to be very efficient for complex materials as demonstrated in many published papers [16,17]. The specific convergence criteria used in VASP relaxation are as follows: (1) the PAW-PBE potentials [18,19] with the generalized gradient approximation (GGA) is used. (2) The electronic convergence criterion is set at 10^{-5} eV. (3) The force convergence criterion is set at 10^{-3} eV/Å for ionic relaxation. (4) A high energy cutoff of 600 eV is adopted and (5) considering the large size of the cell and number of atoms it contains, only one K-point at Γ (0, 0, 0) is used for Brillouin-Zone (BZ) integration.

OLCAO is an all-electron method that uses atomic orbitals expanded in terms of contracted Gaussian-type orbitals (GTOs). The economic use of localized atomic orbitals and efficient evaluation of all multi-center integrals make it especially suitable for complex materials, balancing the size of the system being treated and the required accuracy needed [16]. The local density approximations (LDA) is used for the exchange-correlation potential. The basic electronic structure properties such as total density of state (TDOS), atom- and orbital-resolved partial density of states (PDOS) can be easily obtained. An important parameter in this study is the evaluation of bond order (BO) value or the overlap population ($\rho_{\alpha\beta}$) between any pair of atoms (α, β), based upon the Mulliken population analysis scheme [20]:

$$\rho_{\alpha\beta} = \sum_{n,occ}\sum_{i,j} C^{*n}_{i\alpha} C^{n}_{j\beta} S_{i\alpha,j\beta} \tag{1}$$

where i, j label the orbital quantum number and n the band index, $C^{n}_{j\beta}$ are the eigenvector coefficients of the wave function and $S_{i\alpha,j\beta}$ is the overlap matrix between atoms α and β [16]. BO calculation uses a minimal basis (MB) set which consists of only occupied atomic orbital shell and provides a more localized basis for such analysis.

The self-consistent field (SCF) portion of the OLCAO calculation uses a full basis (FB) set which consists of the MB plus an additional unoccupied shell of orbitals. The optical properties of a-GeO_2 are calculated in the form of the frequency-dependent complex dielectric function and the refractive index n which are important properties of glassy materials [16]. An extended basis (EB) set is usually adopted which an additional shell of unoccupied atomic orbitals in the basis has set beyond the FB. For the calculation of interband optical properties, the imaginary part of the dielectric function ε_2 is evaluated first, using [16]:

$$\varepsilon_2(\hbar\omega) = \frac{e^2}{\pi m\omega^2}\int_{BZ} dk^3 \sum_{n,l} \left|\left\langle \psi_n\left(\vec{k},\vec{r}\right)\left| -i\hbar\,\vec{\nabla}\right|\psi_l\left(\vec{k},\vec{r}\right)\right\rangle\right|^2 f_l\left(\vec{k}\right)\left[1-f_n\left(\vec{k}\right)\right]\delta\left(E_n\left(\vec{k}\right)-E_l\left(\vec{k}\right)-\hbar\omega\right) \tag{2}$$

where $E = \hbar\omega$ is the photon energy, l and n label the occupied and unoccupied states respectively. $\psi_n(\vec{k},\vec{r})$ is the Bloch wave function for the nth band with energy $E_n(\vec{k})$ at Brillouin zone point k; $f(\vec{k})$ is the Fermi distribution function. The momentum matrix elements (MME) $\langle\psi_n(\vec{k},\vec{r})|\vec{P}|\psi_l(\vec{k},\vec{r})\rangle$ are explicitly calculated from the ab initio wave functions. In the present study of a large glass model, only the $\boldsymbol{k} = (0, 0, 0)$ is used. The real part of the dielectric function ε_1 is obtained from the imaginary part ε_2 via Kramers–Kronig transformation [21]:

$$\varepsilon_1(\hbar\omega) = 1 + \frac{2}{\pi}P\int_0^{\infty}\frac{s\varepsilon_2(\hbar\omega)}{s^2-\omega^2}ds. \tag{3}$$

From the complex dielectric function, n can be estimated from the square root of ε_1 at zero frequency, or $n = \sqrt{\varepsilon_1(0)}$.

3. Results and discussion

The periodic CRN model for a-GeO_2 contains 1296 atoms or 432 GeO_2 molecules without any broken bonds or over/under-coordinated Ge or O atoms (Fig. 1). The genesis of this GeO_2 model dates back to the nearly-perfect a-SiO_2 model of the same size that was constructed 20 years ago [9]. This model was obtained from a smaller seed model (162 atoms) that was created even earlier [22] by inserting oxygen atoms in between the Si—Si bonds of a hand-built amorphous Si model followed by rescaling and relaxing using Keating type potentials [22]. Over the last 20 years, this 1296-atom model was systematically improved, refined, and used to study a range of structural and electronic properties of a-SiO_2 as an example of a near-perfect CRN structure for non-crystalline solids [9–12]. Here, we use this model for studying the structure and properties of a-GeO_2 by replacing Si atoms with Ge atoms and fully optimizing the geometry via VASP. We discuss the results below and also compare them with those of the a-SiO_2 model.

3.1. Atomic structure and network bonding

Table 1 lists the final relaxed cell parameters for a-GeO_2 and a-SiO_2 together with the average values of the bond length (BL) and bond angles (BA). The experimental data for a-SiO2 is from Mozzi and Warren which agrees well with our simulated data for the averaged Si—O—Si bridging angle which may be a little lower than from later measurements. The simulated a-GeO_2 model has a density of 3.351 g/cm^3 which is close to the experimental value of 3.69 ± 0.02 g/cm^3 [23]. The calculated pair distribution function (PDF) g(r) for this model is shown in Fig. 2 together with that of a-SiO_2. It also shows the measured X-ray diffraction data from Salmon et al. [24] for a-GeO_2 and that there

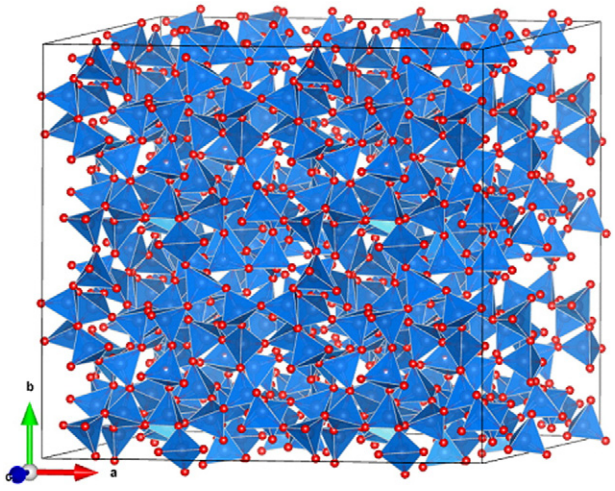

Fig. 1. Ball & stick figure of a continuous random network (CRN) model of a-GeO_2 glass with 432 GeO_2 tetrahedral units (1296 atoms) (purple = Ge, red = O).

Table 1
Physical characteristics of the CRN models for a-AO_2 (A = Ge, Si). Available experimental values are given in parenthesis.

Characteristic	a-GeO_2	a-SiO_2
No. of atoms	1296	1296
a (Å)	28.73	27.44
b (Å)	26.35	25.37
c (Å)	29.65	28.31
α^0	91.07	91.03
β^0	93.99	93.63
γ^0	89.66	90.04
Volume (Å^3)	22,387.45	19,692.16
Density (g/cm^3)	3.351 (3.69[c])	2.202 (2.20[a])
Average BL (Å)	1.790 (1.73[d])	1.631 (1.639[b])
Average O—A—O (θ)	108.71 (109[d])	109.09 (109.47[b])
Average A—O—A (φ)	131.84 (132[d])	145.31 (145.00[b])

Ref. (a) = [48], Ref. (b) = [49], Ref. (c) = [23], Ref. (d) = [24].

is reasonably good agreement with our model. However, our a-GeO_2 model shows a slightly larger BL than the experiment as indicated by the positions of the first peaks in the Ge—O, Ge—Ge, and O—O partial PDF. This could partly be due to the GGA exchange-correlation functional. Many past studies show that GGA overestimates the lattice parameters, volumes, and bond lengths [25].

The SRO in the CRN model is best described by the BL and BA distributions. In Fig. 3(a)–(c), we display the histogram plots for the BL, tetrahedral BA (θ) and bridging BA (φ). The left column is for a-GeO_2 and the right column is for a-SiO_2. They all exhibit an approximate Gaussian distribution but with considerable differences in the mean values and standard root-mean square deviations (σ). The mean Ge—O BL is 1.790 Å with a σ of 0.121 Å compared to the mean Si—O BL of 1.631 Å with a σ = 0.118 Å in a-SiO_2. This is consistent with the fact that the relaxed volume of a-GeO_2 (22,387.45 Å^3) is much larger than the volume for a-SiO_2 (19,668.17 Å^3). The distributions for the BA θ and φ show much larger differences between the two phases. The mean BA and σ values for θ and φ in a-GeO_2 are (108.77°, 10.19°) and (130.99° and 17.05°) respectively. The corresponding values for a-SiO_2 are (109.12°, 9.17°) and (145.26°, 26.89°) respectively. Thus the tetrahedral angle in a-SiO_2 is closer to the perfect tetrahedral angle than in a-GeO_2. These values are listed in Table 1 together with the reported experimental values for comparison [1].

3.2. Electronic structure

Before we present the results on the electronic structure of a-GeO_2, we first show our calculation for the hexagonal crystalline quartz phase (c-GeO_2). The calculated band structure and total density of state (TDOS) and its orbital components are shown in Fig. 4(a) and (b). The result for the DOS is similar to that reported in [26], and differs from that of crystalline SiO_2 (c-SiO_2) [27–30]. The calculated DOS and PDOS for c-GeO_2 are also consistent with the work of Carbret et al. used for the interpretation of the XANES spectra for c-GeO_2 [31]. The TDOS and PDOS for a-GeO_2 and a-SiO_2 are shown in Fig. 5(a) and (b) respectively. The DOS for a-GeO_2 is more broadened than the c-GeO_2 because of the variations in SRO and the lack of LRO in a-GeO_2. A-GeO_2 has a smaller band gap of (2.42 eV) compared to c-GeO_2 (2.66 eV) and also the a-SiO_2 (5.37 eV). The calculated band gaps in both crystalline and amorphous phases of GeO_2 and SiO_2 are underestimated mainly due to the shortcoming of LDA in the DFT for the ground state calculations. However, there are other factors that also affect the comparison between calculated and measured gap values such as the difference between the intrinsic gap from the calculation and extrapolated gap from experiment; the possibility of symmetry restricted transition at the band extremes in crystalline phases, the presence or absence of an excitonic peak near the conduction band (CB) edge, the difference between different methods of calculations, etc. The comparison of reported band gap values of crystalline and amorphous phases for GeO_2 and SiO_2 is shown in Table 2. Compared to the reported experimental values, both c-GeO_2 and c-SiO_2 are underestimated roughly by about 2.9 eV. The band gap of c-SiO_2 is better represented mainly because Si does not contain the occupied 3*d* orbitals whereas Ge has the 3d electrons in the semi-core orbital [32]. Our calculated band gap for c-GeO_2 is somewhat different from other existing calculations. The calculations reported by Broqvist et al. [26] using a hybrid functional PBE + HF show a closer agreement with ours while Christie et al. [33], and others [28,29,34] got closer values to the experimentally observed values [34–36]. These calculations all used pseudopotential plane-wave methods. However, it is interesting to note that although these previous studies got closer agreement for c-GeO_2, they still consistently underestimated the band gap in c-SiO_2 [29] compared to the experiment [34]. This accentuates the fact that the interpretation of the calculated band gaps in both crystalline and amorphous phases of GeO_2 and SiO_2 and their comparison with measured values can be very intricate and need to be extremely cautious.

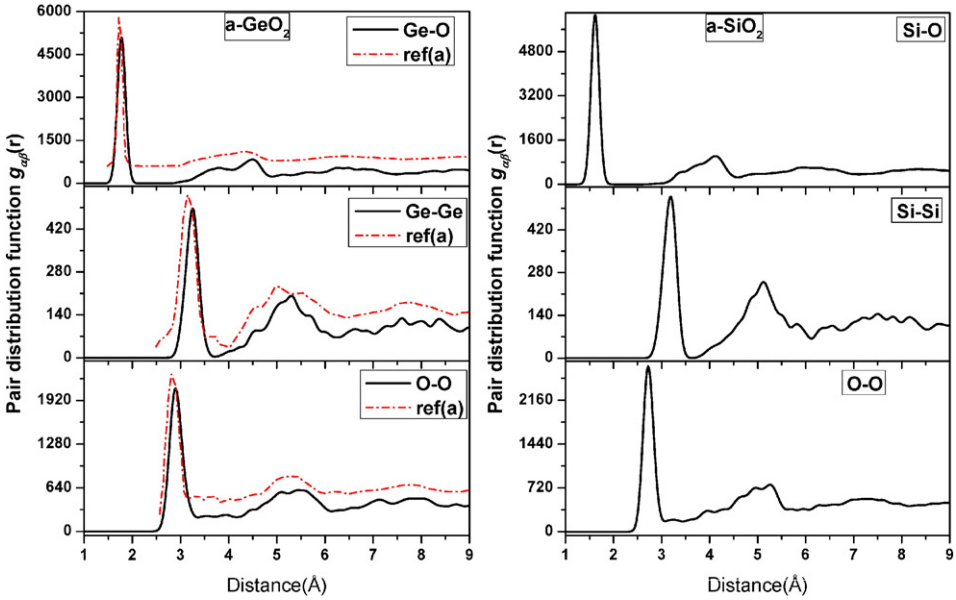

Fig. 2. Radial pair distributions of: (a) a-GeO_2 the (dotted lines are respective experimental RPDF from Ref. (a) = [24]) and (b) a-SiO_2.

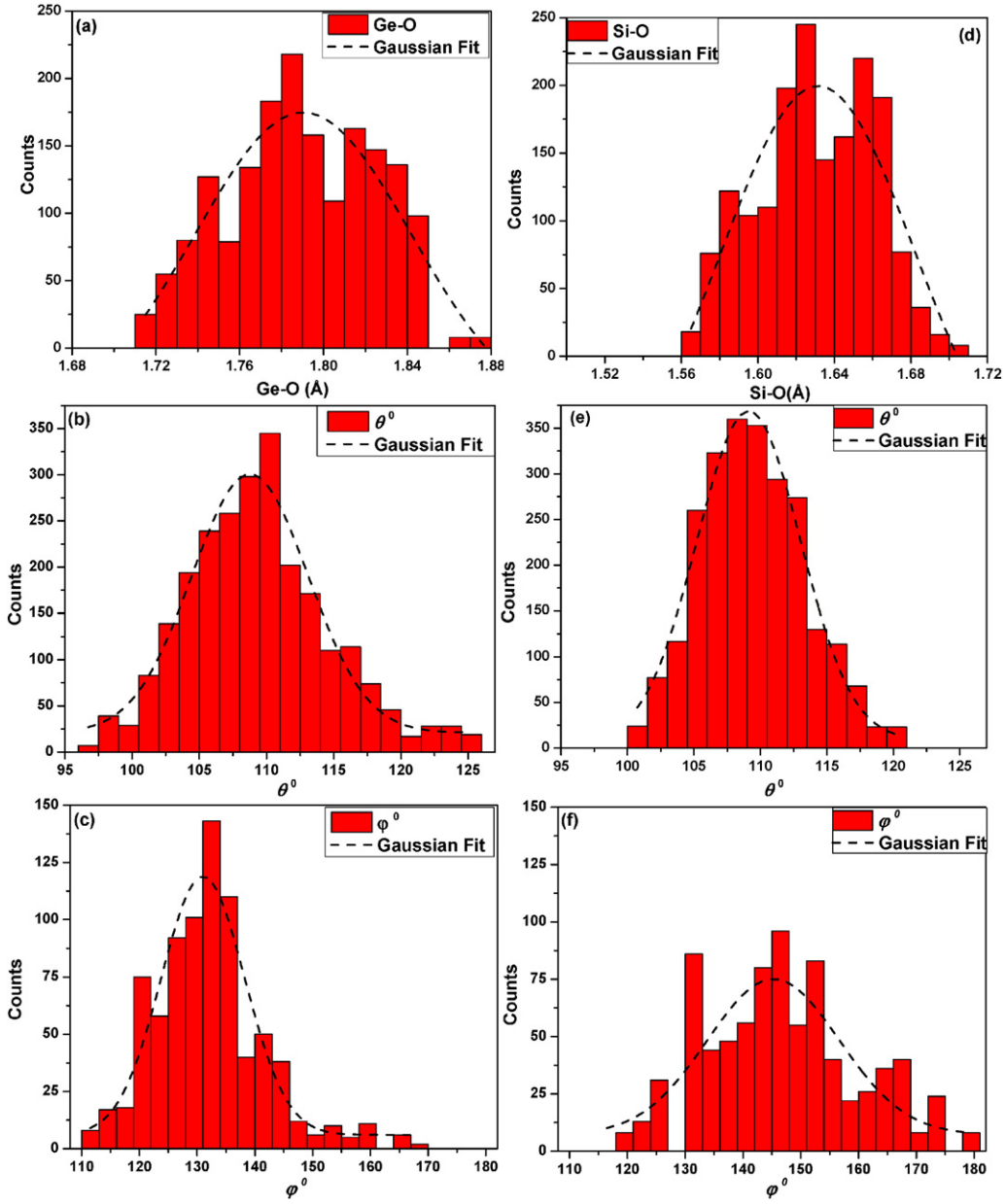

Fig. 3. Distribution of (a) Ge—O bond length, (b) tetrahedral angle θ and (c) bridging angle φ for a-GeO_2. Distribution of (d) Si—O bond length, (e) tetrahedral angle θ and (f) bridging angle φ for a-SiO_2. The Gaussian fit for the distributions is given by dashed lines.

The main features of the TDOS for a-GeO_2 in Fig. 5(a) are the deeper O-2s states (*p*1, *p*2) and various peak structures in the lower (*p*3–*p*5) and upper (*p*6, *p*7) parts of the valence band (VB). These features are quite similar to those in a-SiO_2 (Fig. 5(b)). The main difference is that the upper VB peaks (*p*6 and *p*7) are much more resolvable in a-SiO_2 than in a-GeO_2. The peak structures in the CB region of a-GeO_2 and a-SiO_2 are also quite different which certainly leads to the difference in the optical spectra to be discussed later.

The bond order (BO) value (in unit of electrons e^-) is a measure of the strength of a bond between atoms which in turn can be used to characterize the degree of internal cohesion in a material [17]. Fig. 6(a) and (b) shows the histogram distribution of the BO values for a-GeO_2 and a-SiO_2. They can be represented by a near-perfect Gaussian distribution which is a manifestation of the near perfect bonding features in the a-GeO_2 CRN model. In a-GeO_2, the BO distribution peaks at 0.253 e^- with a standard deviation of 0.019e^-. The corresponding values for a-SiO_2 are 0.281 e^-, 0.020 e^-. Thus a-SiO_2 has stronger bonding and similar distributions as a-GeO_2.

The total bond order density (TBOD) is obtained by summing all the BO pairs and normalizing the cell volume. TBOD is a single parameter from the electronic structure that reflects the internal cohesion of complex materials [37]. The TBOD for a-GeO_2 and a-SiO_2 is 0.01949 $e^-/Å^3$ and 0.0247 $e^-/Å^3$ respectively. They are both smaller than the TBOD of their crystalline counterparts of 0.02318 $e^-/Å^3$ and 0.02808 $e^-/Å^3$ indicating the higher cohesion in crystalline phases than in the amorphous phase and the internal cohesion in silica is stronger than in germania. This is another solid evidence in using TBOD as a single quantum mechanical metric in assessing material properties in both crystalline and non-crystalline solids.

3.3. Optical properties

The most important application for germania is in optics especially in fiber optics [2]. Knowledge of optical properties is important for good glass formers such as germania and silica [1]. We first show the results for c-GeO_2 to facilitate discussion. Fig. 7 shows calculated $\varepsilon_2(\omega)$ for

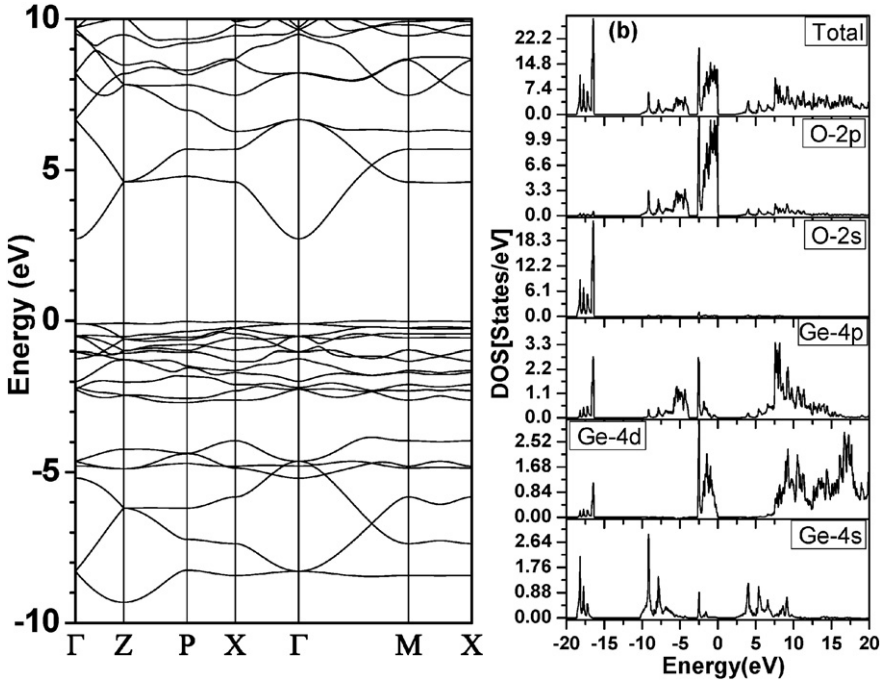

Fig. 4. Calculated (a) band structure and (b) TDOS and orbital resolved PDOS of c-GeO_2.

the c-GeO_2 together with the measured spectra by Pajasova et al. [38]. Incidentally, a 1993 paper by Trukhin suggested the presence of the peak at 6.6 eV based on luminescence data as the evidence of an excitonic peak [39]. It is quite obvious that the observed peaks ***a***, ***b***, ***c*** and ***d*** in Fig. 7 are faithfully reproduced by our calculation. It should be noted that due to the underestimation of the band gap discussed earlier, the experimental spectrum in Fig. 7 is shifted to the left by 1.8 eV. The minor difference in the relative intensities of the peaks could be due to the surface effects of the samples used in the experiment. From $\varepsilon_1(\omega)$, we extracted the refractive index n to be 1.691 which is quite close to the experimental value of 1.64 [40] for crystalline quartz-GeO_2. The experimental $\varepsilon_2(\omega)$ spectra do not show an excitonic peak.

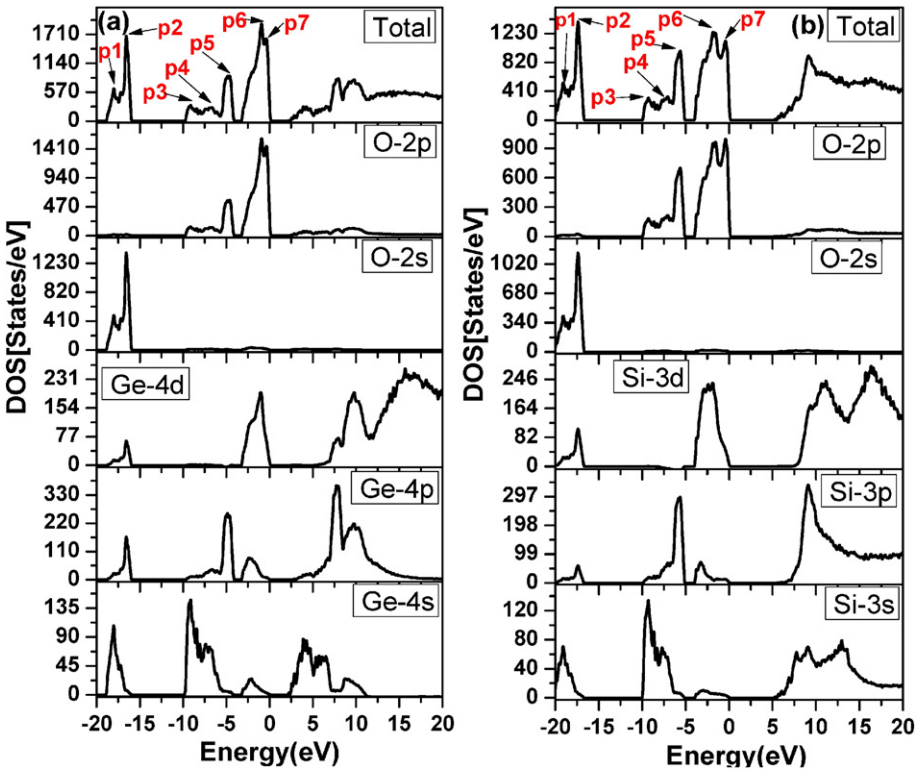

Fig. 5. Calculated TDOS and orbital resolved PDOS of (a) a-GeO_2 and (b) a-SiO_2.

Table 2
Band-gap (eV) for crystalline and amorphous GeO_2 and SiO_2.

	Present work	Other calculations	Experiments
c-GeO_2	2.66	3.2[a], 5[b], 4.34[c]	5.81[d], 5.6[e]
a-GeO_2	2.42	2.8[a], 4.33[e]	5.95[f], 5.6[e]
c-SiO_2	5.37[g]	5.6[g], 5.78[c]	8.3–9.0[e]
a-SiO_2	5.16[g]	5.69[e]	8.7–9.4[e]

Ref. (a): [26], Ref. (b): [33], Ref. (c): [29], Ref. (d): [35], Ref. (e): [34], Ref. (f): [36], Ref. (g): [28].

It is conceivable that an exciton peak in c-GeO_2 may exist but could be merged with or masked by interband absorption peak in the relevant energy range as argued by Trukhin [39].

Fig. 8(a) and (b) show the calculated real and imaginary parts of the dielectric function ($\varepsilon = \varepsilon_1 + i\varepsilon_2$) for a-$GeO_2$ and a-SiO_2 respectively. Our calculation used an improved version of the program in the OLCAO method related to optical transitions at higher energy ranges which is more accurate than used in the previous calculations for the same a-SiO_2 model [11]. For a-GeO_2 shown in Fig. 8(a), the blue dotted line is experimental curve for $\varepsilon_2(\omega)$ from [38]. It shows very good agreement with our calculation. The experimental ε_2 curve is also shifted by 1.8 eV to the left to align with the calculated peak ***l*** to account for the gap underestimation. The $\varepsilon_2(\omega)$ has a steep rise at the threshold 2.7 eV and two major peaks ***l*** (5.2 eV) and ***m*** (9.4 eV) matching well with Pajasová's data [38,41]. The calculated spectrum also shows two minor peak features ***n*** and ***o*** at 10.5 eV and 12.7 eV but they are not sufficiently resolved in the experimental curve. Although the experimental spectrum was known for some time, no interpretation has been given [42]. Instead, comparison to the crystalline hexagonal GeO_2 was given by Pajasová [38]. The major $\varepsilon_2(\omega)$ peaks for crystal and glass phases shown in Figs. 7 and 8(b) are quite similar confirming the similarity in the SRO in both phases as already discussed above. In c-GeO_2, there are more structures in the range near the first major peak. This is due to the crystalline phase having LRO with sharper peak structures in the DOS.

In contrast to a-GeO_2, the optical absorption spectra of a-SiO_2 have been studied quite extensively both theoretically and experimentally

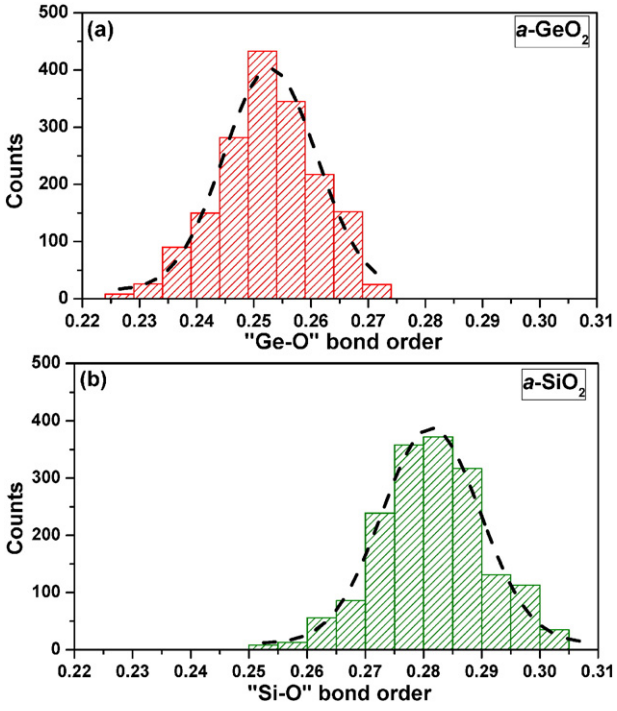

Fig. 6. Ge—O bond order distribution of (a) a-GeO_2 and (b) a-SiO_2.

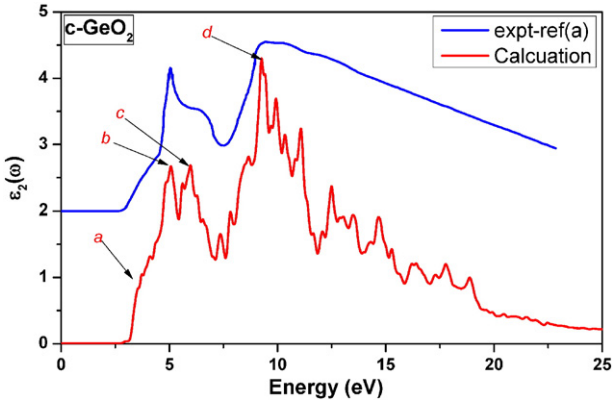

Fig. 7. Calculated (red) and experimentally measured (blue, Ref. [37]) imaginary part of the complex dielectric function for c-GeO_2.

[11,28,30,43,44] but full interpretation of peak structures is still lacking [11]. Here, we attempt to analyze the optical properties of SiO_2 in-depth so as to have a better understanding of the origin of the peak structures in the absorption spectrum. The experimental data for a-SiO_2 by Tarrio et al. [45] shown in Fig. 8(b) agree with our calculation quite well apart from the presence of an excitonic peak which cannot be obtained by DFT calculation using the one-electron approach. The experimental curve is shifted downward by 2.37 eV to match with calculated peaks (see vertical dashed lines) for two reasons. First, the actual absorption edge onset is marked by the excitonic peak ***q***. Second, DFT calculations underestimate the bandgap. With our recent effort to improve the

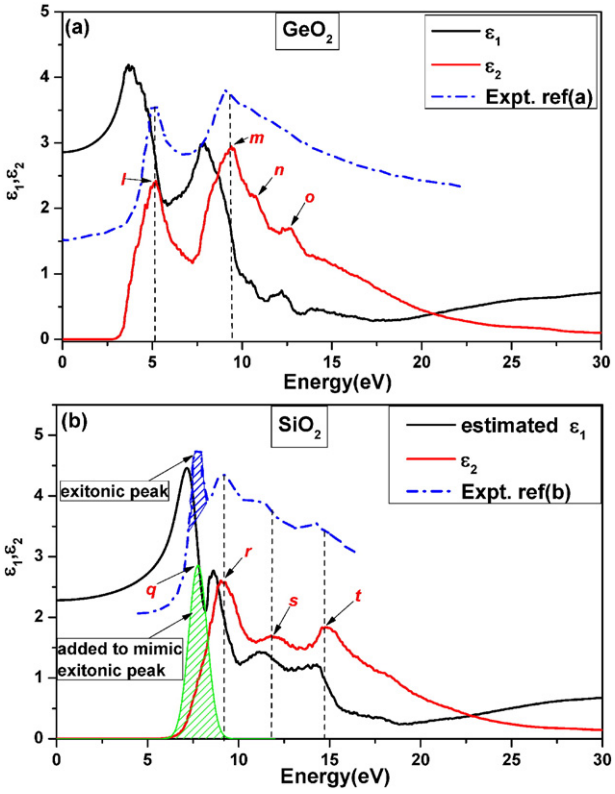

Fig. 8. Calculated real and imaginary parts of the dielectric function for (a) a-GeO_2 and (b) a-SiO_2. The experimental data (dashed line) for $\varepsilon_2(\omega)$ is from Ref. (a) [39] and Ref. (b) [43].

optical property calculation at higher frequency range, the agreement of ε_2 with experiment is better than our previously published results [10,11]. This can be seen from the positions of three peaks ***r***, ***s***, and ***t*** at energies 9 eV, 11.8 eV, and 14.8 eV respectively in Fig. 8(b). The refractive index n of 1.455 obtained from $\varepsilon_1(0)$ for a-SiO_2 without the excitonic peak is very close to the generally acceptable value of 1.458 for amorphous silica [46]. However, the measured refractive index value depends on experimental conditions and the frequency of incident radiation. It can be in the range of 1.42 to 1.55 eV [47]. The reported refractive index n for crystalline quartz SiO_2 is 1.554 [46], which is larger than a-SiO_2.

The present calculation of optical properties using the OLCAO method does not account for the presence of the excitonic peak which is observed in both crystalline and amorphous SiO_2. The refractive index will be affected by the presence of the excitonic peak in $\varepsilon_2(\omega)$ because $\varepsilon_1(\omega)$ is obtained from KKR conversion of $\varepsilon_2(\omega)$. To ascertain the difference in the refractive index due to the negligence of the excitonic peak, we added a simulated Gaussian peak that has the same width and position as the experimentally observed peak to mimic the effect of the excitonic peak. This is shown as the shaded green peak in Fig. 8b. From this modified $\varepsilon_2(\omega)$ and the subsequent $\varepsilon_1(\omega)$ obtained using KK conversion, we obtained a refractive index of 1.51. This still falls in the acceptable range of n of a-SiO_2. So far, the calculation does not account for the underestimation of band gap. If this effect is also accounted for then the calculated refractive index of 1.455 (1.51) with (without) the excitonic peak will be slightly reduced, giving the latter a value that is closer to the experimental value. Thus, it is possible to account for the excitonic effect by adding a simulated peak to the results from a conventional one-electron calculation without invoking much more complicated many body corrections in systems such as a-SiO_2.

4. Conclusion

In conclusion, we report the results of electronic structure and optical property calculations for a large CRN model for a-GeO_2 using accurate ab initio methods. Similar results for the a-SiO_2 model of the same size and the crystalline GeO_2 are used for comparison and interpretation of the optical data. The BL and BO distributions have a Gaussian type distribution reflecting the nearly-perfect coordinated models. The a-GeO_2 model has a broad θ distribution and a slightly skewed symmetric Gaussian distribution for φ, which is narrower than the respective distribution for a-SiO_2. Also, a-GeO_2 has a smaller band gap compared to silica and a lower mean BO compared to a-SiO_2 [11]. The difference in the electronic structure between a-GeO_2 and a-SiO_2 is reflected in the calculated TDOS due to the different atomic configurations and sizes of Ge and Si atoms. The calculated refractive index for a-GeO_2 is 1.691 which is close to the experimental value of 1.64 for quartz c-GeO_2. By adding an ad hoc excitonic peak to the calculated absorption curve for a-SiO_2, we show that the estimated refractive index for a-SiO_2 can be improved. The present study can be further extended to other related glass models such as composite mixtures of a-SiO_2 and a-GeO_2, models containing specific defects or intentional doping in glasses, and even with vitreous nano-particles. It can also be used for targeted study of specific defective structures or inclusion of intentionally doped impurities. It is also important to perform further experiments in elucidating the possible existence of exciton in both c-GeO_2 and a-GeO_2.

Acknowledgments

WYC is supported by the U.S. DOE, Office of Basic Energy Sciences, Division of Material Science and Engineering under Award DE-SC008176. This research used the resources of the National Energy Research Scientific Computing Center supported by the DOE under Contract No. DE-AC03-76SF00098.

References

[1] M. Micoulaut, L. Cormier, G. Henderson, The structure of amorphous, crystalline and liquid GeO_2, J. Phys. Condens. Matter 18 (45) (2006) R753.
[2] E.M. Dianov, V.M. Mashinsky, Germania-based core optical fibers, J. Lightwave Technol. 23 (11) (2005) 3500–3508.
[3] M. Wysokowski, et al., Extreme biomimetic approach for development of novel chitin–GeO_2 nanocomposites with photoluminescent properties, Nano Res. 8 (7) (2015) 2288–2301.
[4] S. Valligatla, et al., CO_2 laser irradiation of GeO_2 planar waveguide fabricated by RF-sputtering, IOP Conference Series: Materials Science and Engineering, IOP Publishing, 2015.
[5] S. Sebastiani, et al., Characterization of a highly photorefractive RF-sputtered SiO_2–GeO_2 waveguide, Opt. Express 13 (5) (2005) 1696–1701.
[6] A. Anan'ev, et al., Origin of Rayleigh scattering and anomaly of elastic properties in vitreous and molten GeO_2, J. Non-Cryst. Solids 354 (26) (2008) 3049–3058.
[7] A.N. Rosli, et al., Clusters of Ge and O atoms and the Raman spectra of vitreous GeO_2, AIP Conference Proceedings—American Institute of Physics, 1328(1) 2011, p. 71.
[8] C.C. Dharmawardhana, DFT Calculations of Vibrational Modes of Arsenic Sulfide and Phosphorus Sulfide Glass, Central Michigan University, 2007.
[9] M.-Z. Huang, W.Y. Ching, Electron states in a nearly ideal random-network model of amorphous SiO_2 glass, Phys. Rev. B Condens. Matter 54 (8) (1996) 5299–5308.
[10] M.-Z. Huang, L. Ouyang, W.Y. Ching, Electron and phonon states in an ideal continuous random network model of a-SiO_2 glass, Phys. Rev. B Condens. Matter 59 (5) (1999) 3540–3550.
[11] N. Li, W.-Y. Ching, Structural, electronic and optical properties of a large random network model of amorphous SiO_2 glass, J. Non-Cryst. Solids 383 (2014) 28–32.
[12] N. Li, et al., Densification of a continuous random network model of amorphous SiO_2 glass, Phys. Chem. Chem. Phys. 16 (4) (2014) 1500–1514.
[13] G. Kresse, J. Hafner, Ab initio molecular dynamics for liquid metals, Phys. Rev. B 47 (1) (1993) 558–561.
[14] G. Kresse, J. Furthmüller, Efficiency of ab-initio total energy calculations for metals and semiconductors using a plane-wave basis set, Comput. Mater. Sci. 6 (1) (1996) 15–50.
[15] W.Y. Ching, Theoretical studies of the electronic properties of ceramic materials, J. Am. Ceram. Soc. 73 (11) (1990) 3135–3160.
[16] W.Y. Ching, P. Rulis, Electronic Structure Methods for Complex Materials: The Orthogonalized Linear Combination of Atomic Orbitals, Oxford University Press, USA, 2012 360.
[17] C.C. Dharmawardhana, et al., Role of interatomic bonding in the mechanical anisotropy and interlayer cohesion of CSH crystals, Cem. Concr. Res. 52 (2013) 123–130.
[18] P.E. Blöchl, Projector augmented-wave method, Phys. Rev. B 50 (24) (1994) 17953–17979.
[19] J.P. Perdew, Accurate density functional for the energy: real-space cutoff of the gradient expansion for the exchange hole, Phys. Rev. Lett. 55 (16) (1985) 1665–1668.
[20] R.S. Mulliken, Electronic population analysis on LCAO—MO molecular wave functions. I, J. Chem. Phys. 23 (10) (1955) 1833–1840.
[21] P.C. Martin, Sum rules, Kramers–Kronig relations, and transport coefficients in charged systems, Phys. Rev. 161 (1) (1967) 143.
[22] W.Y. Ching, Microscopic calculation of localized electron states in an intrinsic glass, Phys. Rev. Lett. 46 (9) (1981) 607–610.
[23] M. Akaogi, et al., Enthalpy and density measurements of pressure-amorphized GeO_2 quartz, Geophys. Res. Lett. 25 (19) (1998) 3635–3638.
[24] P.S. Salmon, et al., Structure of glassy GeO_2, J. Phys. Condens. Matter 19 (41) (2007) 415110.
[25] A. van de Walle, G. Ceder, Correcting overbinding in local-density-approximation calculations, Phys. Rev. B 59 (23) (1999) 14992–15001.
[26] P. Broqvist, J.F. Binder, A. Pasquarello, Band offsets at the Ge/GeO_2 interface through hybrid density functionals, Appl. Phys. Lett. 94 (14) (2009) (141911-141911-3).
[27] Y.N. Xu, W.Y. Ching, Comparison of charge-density distribution and electronic bonding in silica and silicon nitride (alpha-SiO_2 and beta-Si_3N_4), Physica B + C (Amst.) 150 (1–2) (1988) 32–36.
[28] W.Y. Ching, First principles calculation of the electronic structures of crystalline and amorphous forms of SiO_2, Struct. Imperfections Amorphous Cryst. Silicon Dioxide2000 167–179.
[29] C. Sevik, C. Bulutay, Theoretical study of the insulating oxides and nitrides: SiO_2, GeO_2, Al_2O_3, Si_3N_4, and Ge_3N_4, J. Mater. Sci. 42 (16) (2007) 6555–6565.
[30] S. Nekrashevich, V. Gritsenko, Electronic structure of silicon dioxide (a review), Phys. Solid State 56 (2) (2014) 207–222.
[31] D. Cabaret, F. Mauri, G.S. Henderson, Oxygen K-edge XANES of germanates investigated using first-principles calculations, Phys. Rev. B 75 (18) (2007) 184205.
[32] N. Binggeli, et al., Electronic properties of alpha-quartz under pressure, Phys. Rev. B 44 (10) (1991) 4771–4777.
[33] D.M. Christie, J.R. Chelikowsky, Electronic and structural properties of germania polymorphs, Phys. Rev. B 62 (22) (2000) 14703–14711.
[34] T. Tamura, et al., First-principles study of neutral oxygen vacancies in amorphous silica and germania, Phys. Rev. B 69 (19) (2004) 195204.
[35] M. Perego, et al., Fabrication of GeO_2 layers using a divalent Ge precursor, Appl. Phys. Lett. 90 (16) (2007) (162115–162115-3).
[36] T. Lange, et al., Physical properties of thin GeO_2 films produced by reactive DC magnetron sputtering, Thin Solid Films 365 (1) (2000) 82–89.
[37] C.C. Dharmawardhana, A. Misra, W.Y. Ching, Quantum mechanical metric for internal cohesion in cement crystals, Sci. Rep. 4 (2014) 7332.
[38] L. Pajasova, Optical properties of GeO_2 in the ultraviolet region, Czechoslov. J. Phys. B 19 (10) (1969) 1265–1270.

[39] A.N. Trukhin, Luminescence of a self-trapped exciton in GeO_2 crystal, Solid State Commun. 85 (8) (1993) 723–728.
[40] J.W. Fleming, Dispersion in GeO_2–SiO_2 glasses, Appl. Opt. 23 (24) (1984) 4486–4493.
[41] L. Pajasova, et al., Optical properties of reactively sputtered GeO_2 in the vacuum ultraviolet region, J. Non-Cryst. Solids 182 (3) (1995) 286–292.
[42] N. Ravindra, R. Weeks, D. Kinser, Optical properties of GeO_2, Phys. Rev. B 36 (11) (1987) 6132.
[43] G.-L. Tan, M.F. Lemon, R.H. French, Optical properties and London dispersion forces of amorphous silica determined by vacuum ultraviolet spectroscopy and spectroscopic ellipsometry, J. Am. Ceram. Soc. 86 (11) (2003) 1885–1892.
[44] G.L. Tan, et al., Optical properties and London dispersion interaction of amorphous and crystalline SiO_2 determined by vacuum ultraviolet spectroscopy and spectroscopic ellipsometry, Phys. Rev. B 72 (20) (2005) 205117.
[45] C. Tarrio, S. Schnatterly, Optical properties of silicon and its oxides, J. Opt. Soc. Am. B 10 (5) (1993) 952–957.
[46] R.C. Weast, CRC Handbook of Chemistry and Physics, 68th Edition, vol. 68, CRC Press 1988, p. 1760.
[47] E.D. Palik, Handbook of Optical Constants of Solids, Elsevier Science, 2012.
[48] S.R. Elliott, Physics of Amorphous Materials, Longman Scientific & Technical, 1990.
[49] R. Mozzi, B. Warren, The structure of vitreous silica, J. Appl. Crystallogr. 2 (4) (1969) 164–172.